frontiers | Frontiers in Environmental Science

TYPE Original Research
PUBLISHED 06 August 2025
DOI 10.3389/fenvs.2025.1615815

OPEN ACCESS

EDITED BY
Ahmed El Nemr,
National Institute of Oceanography and Fisheries (NIOF), Egypt

REVIEWED BY
Nurasmat Shukri,
Universiti Sains Malaysia Health Campus, Malaysia
Md. Rajibul Akanda,
Jagannath University, Bangladesh

*CORRESPONDENCE
Nada El Darra,
n.aldarra@bau.edu.lb

RECEIVED 21 April 2025
ACCEPTED 03 July 2025
PUBLISHED 06 August 2025

CITATION
Helmi L, Sunoqrot S, Hijazi A, Alayli M, Rajha HN, Al Bakri M, El-Dakdouki MH and El Darra N (2025) Tomato leaves as a sustainable biosorbent for the effective removal of some organic dyes and lead from water.
Front. Environ. Sci. 13:1615815.
doi: 10.3389/fenvs.2025.1615815

Tomato leaves as a sustainable biosorbent for the effective removal of some organic dyes and lead from water

Layan Helmi[1], Suhair Sunoqrot[2], Akram Hijazi[3], Maria Alayli[4], Hiba N. Rajha[5], Maram Al Bakri[4], Mohammad H. El-Dakdouki[6] and Nada El Darra[4]*

[1]Department of Biological Sciences, Faculty of Science, Beirut Arab University, Beirut, Lebanon, [2]Faculty of Pharmacy, Al-Zaytoonah University of Jordan, Amman, Jordan, [3]Doctoral School of Science and Technology, Research Platform for Environmental Science (PRASE), Lebanese University, Beirut, Lebanon, [4]Department of Nutrition and Dietetics, Faculty of Health Sciences, Beirut Arab University, Beirut, Lebanon, [5]Département de Génie Chimique et Pétrochimique, Faculté d'Ingénierie, Ecole Supérieure d'Ingénieurs de Beyrouth (ESIB), Université Saint-Joseph de Beyrouth, Beirut, Lebanon, [6]Department of Chemistry, Faculty of Science, Beirut Arab University, Beirut, Lebanon

Introduction: Water, an essential component for life and agriculture, is increasingly threatened by contamination. Industrial wastewater is a major source of pollution that continues to negatively impact ecosystems and human health. It contains contaminants such as dyes, heavy metals, pharmaceuticals, and pesticides, emphasizing the urgent need for effective water purification methods. This study investigates the valorization of tomato leaves as a potential adsorbent for these pollutants.

Methods: Characterization of untreated and contaminant-treated tomato leaves by Fourier transform infrared spectroscopy (FTIR), X-ray diffraction (XRD), and scanning electron microcopy (SEM), confirmed the presence of significant functional group interactions and surface active sites suited for adsorption.

Results: Tomato leaves demonstrated significant adsorption capabilities for contaminants like methylene blue, malachite green, crystal violet, and lead, achieving removal efficiencies of 90.7% $\pm$ 0.3, 93.6% $\pm$ 0.5, 89.8% $\pm$ 0.6, and 78.4% $\pm$ 0.2, respectively, at an initial contaminant concentration of 20 mg/L. High adsorption effectiveness was also observed across various dye concentrations (5-25 mg/L) and contact times (5-120 min). Isotherm analysis indicated that lead adsorption followed the Langmuir model and Henry adsorption isotherm with a maximum adsorption capacity of 45.77 mg/g, while dyes aligned with the Freundlich model, with adsorption kinetics best fitting the pseudo-second order model in all cases.

Discussion: To our knowledge, this is the first study to comprehensively evaluate the adsorption of both heavy metals (Pb^{2+}) and three structurally different cationic dyes using raw, unmodified tomato leaves. This provides a sustainable, cost-effective, and green solution for the removal of diverse pollutants from water.

Future work can explore enhancing the efficiency of decontamination and real-life application, including performing field trials in diverse environmental and industrial wastewater scenarios.

KEYWORDS

adsorption, heavy metals, industrial wastewater, sustainable purification, tomato leaves, water contamination

1 Introduction

Technological advances have brought many comforts and conveniences; however, industrialization has also contributed significantly to environmental pollution, particularly air, soil, and water pollution (Ahmed et al., 2022). This pollution can have severe consequences on the health of human beings and living organisms. Water pollution particularly poses a serious threat as it is an essential and fundamental component of life. Its contamination can lead to water insecurity, thus endangering communities at large. Sources of water contamination include heavy metals, dyes, pesticide residues, among others; these contaminants can adversely impact health by inducing cardiovascular toxicity, endocrine disruption, reproductive toxicity, central nervous system injury, liver damage, and skin irritation (Lin et al., 2022).

Heavy metals are non-biodegradable and tend to bioaccumulate in the human body upon long term exposure to a contaminated source of water. Heavy metals interact with vital cellular components leading to adverse side-effects, as the body struggles to eliminate these toxic substances (Singh et al., 2024). The ions of heavy metals enter water bodies and the environment from different sources, with industrial waste being one of the prime contributors. They may also enter through other sources such as fertilizers, pharmaceuticals, batteries, and pesticides (Bolisetty et al., 2019). Among the deleterious heavy metals, lead is one of the most commonly encountered pollutants in industrial wastewater (Samuel et al., 2018). Lead could pose significant risk to the proper functioning of the kidneys, liver, and the nervous system (Jang and Hwang, 2018). Due to the high toxicity of lead, the U.S. Food and Drug Administration (FDA) has set the permissible limit in bottled drinking water at just 5 ppb or 0.005 mg/L (Lead in Food and Foodwares, 2025), which is well below the permissible limits of other heavy metals such as arsenic (0.01 mg/L), nickel (0.1 mg/L), or zinc (5 mg/L) (Qasem et al., 2021). In Lebanon, the Libnor standard of lead in non-bottled drinking water is 0.01 mg/L (Nl Norme Libanaise Eau Potable Drinking Water, 2025), which is comparable to the level placed by the U.S. Environmental Protection Agency that assigned a limit of 15 ppb (0.015 mg/L) in public drinking water, as it accounts for the lead that may leach from pipes in tap water (Basic Information about Lead in Drinking Water, 2025).

Dyes are another type of contaminants that are often discharged into aquatic systems in the wastewater of several industries. There are many types of dyes including methylene blue (MB), malachite green (MG), and crystal violet (CV) to name a few. Methylene blue is a heterocyclic aromatic compound with a central thiazine ring containing sulfur and nitrogen, with dimethylamino groups on the aromatic rings (Khan et al., 2022). Malachite green is a triphenylmethane dye with an aromatic structure. It has a central carbon atom bonded to three aromatic rings with dimethylamino groups on two of the aromatic rings (Sharma et al., 2023). Crystal violet is similar to malachite green being a triphenylmethane dye with a central carbon atom bonded to three aromatic rings and dimethylamino groups on all three of the aromatic rings (Votat et al., 2024). Such cationic dyes are used as coloring agents for textile, food, paper, and cosmetics in various industries (Sen, 2023). Wastewater containing dyes is considered a major environmental hazard since the color remains visible even at low dye concentrations. In addition, dyes are highly toxic and can pose carcinogenic and mutagenic effects (Lellis et al., 2019). They are chemically stable and resistant to degradation by sunlight and natural bioremediation processes, rendering their removal from water bodies a challenging task (Pham et al., 2023). Therefore, finding new methods for the proper and efficient decontamination of dyes becomes urgent.

Over the past years, many techniques have been studied and employed to remove contaminants from water including membrane filtration (Xiang et al., 2022), photocatalytic degradation (Mubarak et al., 2022; Aljawrneh et al., 2024), precipitation (Kumar et al., 2021), and adsorption (Yin et al., 2017). However, many of these applications have constraints in various countries due to economic reasons. The inherent limitations of these approaches spurred the development of innovative yet efficient and cost-effective technologies for water purification. Among these methods, adsorption is recognized as a physicochemical separation technique that is highly effective and environmentally friendly to treat contaminated water (Elgarahy et al., 2021). Such method is efficient in removing pollutants while being economically friendly. The use of industrial by-products, agricultural waste, and natural materials is gaining popularity as a cost-effective method to treat wastewater (Foroutan et al., 2022). Due to their chemical composition, plant leaves can be a popular choice for adsorption experiments. The leaves contain cellulose, lignin, polyphenols, carbohydrates, and proteins that may act as active sites for contaminant retention (Peydayesh and Rahbar-Kelishami, 2015; Khodabandehloo et al., 2017).

Tomatoes are a widely consumed crop known for its health benefits, attributed to the wide variety of phytochemicals it contains. Phenolic compounds and carotenoids are abundantly present in tomatoes with the red color attributed to lycopene, linked to reducing cancer risk (Martí et al., 2016). It also contains β-carotene known for its provitamin A activity. Although the fruit has been studied for its constituents and phytochemical properties, the leaves, despite being from the same plant, remain significantly underutilized and unexplored. Tomato leaves are considered agricultural by-products of tomato production with estimates suggesting that at least 120 million tons of tomato leaves were produced annually over the past decade (FAOSTAT, 2025). The main composition of the plant includes lignocellulosic materials, which are hemicellulose (20–40 wt%), cellulose (30–60 wt%), and

lignin (10–25 wt%) (Bourmaud et al., 2023). Leaves account for about 40% of the plant mass, thus highlighting the magnitude of organic waste generated during tomato production (Junker-Frohn et al., 2019). Despite this volume, tomato leaves remain underutilized in value-added applications such as wastewater treatment, where most research focused on processing the fruit waste such peels and seeds. They were tested for their adsorption capability against pharmaceuticals—namely dexamethasone, febantel, procaine, praziquantel, and tylosin—from water, demonstrating promising removal efficiency through a spontaneous and predominantly exothermic process, with adsorption kinetics best described by the pseudo-second-order model (Pavlović et al., 2021). Additionally, a study conducted by Tam and coworkers (Tam et al., 2021) tested the efficiency of different parts of the tomato as an antimicrobial agent and reported that the leaves were the most effective in inhibiting all the tested strains without affecting the beneficial *lactobacilli* found in normal flora. Such antimicrobial activity was attributed to the chemical composition of the leaves which showed high levels of α-tomatine and dehydrotomatine, glycoalkaloids that are typically found in tomatoes. As for polyphenols, quercetin glycosides, particularly quercetin rutinoside, and small amounts of chlorogenic acid were detected in tomato leaves. In another study, tomato leaves exhibited remarkable efficiency as an adsorptive material for the removal of nickel from water (Gutha et al., 2015).

The purpose of the current study is to test the capability of tomato leaves, in powder form, to adsorb contaminants that can be commonly found in wastewater. The contaminants chosen included the heavy metal lead, and dyes, namely, methylene blue, malachite green, and crystal violet. The dual focus on organic and inorganic pollutants allows for a broader assessment of biosorption behavior, which better simulates real-life wastewater profiles. Tomato leaves were chosen since it is an abundant agricultural by-product that remain underexplored to see their potential as a natural, cost-effective, and eco-friendly biosorbent. While biochar and chemically modified adsorbents have been widely studied (Tam et al., 2021; Gutha et al., 2015), there remains a gap in assessing the adsorption efficiency of raw agricultural waste under real-world scenarios. Moreover, the use of unmodified biomass reduces processing costs, energy input, and chemical use, aligning with green chemistry principles and sustainable waste valorization frameworks. This study hypothesizes that unmodified tomato leaf powder can serve as an efficient biosorbent for both dyes and heavy metals, emphasizing sustainability, scalability, and minimal processing cost.

2 Materials and methods

2.1 Raw materials and chemicals

The tomato leaves were obtained from the Beqaa Region, Eastern Lebanon, in August of 2023. The leaves were collected fresh through pruning, selecting those no longer needed. Instead of being discarded, they were repurposed for this study. The tomatoes were of the Ammani plum tomato variety. The leaves were received immediately after fruit harvest and then washed twice with distilled water to remove impurities and sundried in a closed area to avoid microbial contamination for 48 h at around 30 °C when exposed to sun. They were then ground into fine powder form with particle size between 0.5 and 1 mm and stored in a cool dry area (refrigerator) until ready to be used. Lead (II) nitrate, Pb^{2+} standard solution of 1000 ppm (mg/L), methylene blue, malachite green, and crystal violet, were purchased from Sigma Aldrich (Steinheim, Germany). All chemicals were analytical grade and used as received from the supplier. Distilled water was used for dye experiments and deionized water was used for lead experiments.

2.2 Experimental setup

The adsorption experiment was adapted from a study done by Baby et al. (2019). A standard solution of 1000 mg/L was prepared for each contaminant by dissolving the appropriate amount in distilled or deionized water. Adsorption experiments were performed in a 250 mL flask containing 100 mL of dye or metal ion solution and shaken at 120 rpm at room temperature (25°C). Tests were performed in triplicate. When investigating the effect of adsorbent amount on adsorption, the other variables were kept constant, and the testing was conducted for 120 min with contaminants having a concentration of 20 mg/L. As for the effect of contact time, the optimized amount of the adsorbent and the concentration of the contaminants were kept constant. For the effect of initial concentration of the contaminant, the amount of adsorbent was fixed, and the contact time was set for 120 min.

Lead samples were filtered using a syringe filter then analyzed by atomic absorption spectrometry (Thermo Scientific iCE 3000 Series Atomic Absorption Spectrometer (AAS), Thermo Scientific, Franklin, MA, United States), while dye samples were filtered using filter paper and analyzed by a UV-Vis spectrophotometer (Gold S54T UV-VIS, China). The absorbance of MB was read at 668 nm (Fito et al., 2023), MG at 618 nm (Deng et al., 2022), and CV at 590 nm (Mulla et al., 2024). Calibration curves were prepared for each contaminant to determine unknown concentrations.

The adsorption efficiency was expressed as the percentage of removal, and was calculated by Equation 1 (Arabkhani and Asfaram, 2020):

$$\%Removal = \frac{C_0 - C_t}{C_0} \times 100 \quad (1)$$

The adsorption capacity (q) was calculated by Equation 2 (Arabkhani and Asfaram, 2020)

$$q = \frac{C_0 - C_t}{m} \times V \quad (2)$$

where C_0 and C_t are the initial and final concentrations of contaminant, respectively (ppm; mg/L), V is the volume of the solution (L), and m is the mass of dry adsorbent (g).

2.3 Lead levels in tomato leaves powder (TLP)

Acid digestion method was employed to check the level of lead in TLP. It was done by adding 7 mL of nitric acid and 1 mL of hydrogen

peroxide and was performed in a high-performance microwave digestion system (Anton Paar, Multiwave 3000, Graz, Austria). The final clear digest was then diluted to 50 mL with ultrapure water and filtered with 4 μm PTFE filters for analysis using AAS (Bizzi et al., 2011).

2.4 Characterization

Tomato leaves powder (TLP), before and after adsorption, was characterized by Fourier Transform Infrared (FTIR) spectroscopy. After adsorption, the wet powder collected post adsorption was dried using a hot air oven before characterization. Individual contaminants (CV, MB, MG, and Pb^{2+}) were also analyzed for comparison. All samples were prepared as KBr discs and analyzed using an IR Affinity-1 spectrometer (Shimadzu, Kyoto, Japan), where the FTIR spectra were scanned between 4000 and 650 cm^{-1}.

X-ray diffraction (XRD) was carried out using a Rigaku MiniFlex 600 instrument (Tokyo, Japan) equipped with Cu Kα radiation. XRD patterns were acquired over a 2θ range from 10° to 80° at a scanning rate of 2°/min and a step size of 0.1°.

Morphological analysis of the adsorbent before and after adsorption was done using JEOL JSM-IT200 scanning electron microscopy (SEM). Samples were sputter coated with platinum and viewed at an accelerating voltage of 10 kV.

2.5 Isotherm model analysis

The adsorption isotherms were studied by keeping the temperature (25°C), contact time (120 min), and adsorbent dosage constant, while varying the initial contaminant concentrations at 5, 10, 15, 20, and 25 ppm (mg/L). The linearized form of Langmuir isotherm is presented as shown in Equation 3 (Marwani et al., 2017):

$$\frac{1}{q_e} = \frac{1}{q_m.K_L.C_e} + \frac{1}{q_m} \tag{3}$$

where q_e is the quantity of adsorbate per adsorbent mass at equilibrium (mg/g), q_m (mg/g) denotes the maximum adsorption capacity for a monolayer on the adsorbent, K_L (L/mg) represents the Langmuir constant associated with the adsorption free energy, while C_e represents the equilibrium adsorbate concentration in the solution. Additionally, R_L, the separation factor constant, is used to evaluate the feasibility of the Langmuir isotherm and denote the nature of adsorption. If $R_L > 1$, the adsorption is considered unfavorable, favorable if $0 < R_L < 1$, or irreversible if $R_L = 0$ (Marwani et al., 2017). R_L is denoted as shown in Equation 4:

$$R_L = \frac{1}{1 + K_L.C_e} \tag{4}$$

As for the Freundlich isotherm model, the linearized form is presented in Equation 5 (Fito et al., 2023):

$$log\, q_e = log\, K_F + \frac{1}{n}\, log\, C_e \tag{5}$$

In this equation, K_F (mg/g) is an indicator of the adsorption capacity and n is the adsorption intensity. If $n > 1$, the adsorption is considered unfavorable, favorable if $0 < n < 1$, or considered linear if $n = 1$ where the amount of contaminant adsorbed is directly proportional to the concentration of contaminant in the solution.

Additionally, Temkin adsorption isotherm was also studied. This isotherm is made upon the assumption that adsorption is a multi-layer process with a consistent distribution of binding energies up to a defined maximum. It also proposes that heat released during adsorption gradually decreases in a linear fashion as surface coverage increases due to the interactions between the adsorbate and adsorbent (Elkhaleefa et al., 2020). The linearized form is presented in Equation 6:

$$q_e = \frac{RT}{b} ln\, K_T + \frac{RT}{b}\, ln\, C_e \tag{6}$$

In this equation, R is the universal gas constant (8.314 J/mol·K), T is the temperature in Kelvin, b is the Temkin constant related to heat of sorption (J/mol) and K_T is the Temkin isotherm constant (L/g).

2.6 Kinetic model analysis

Kinetic analysis was done to determine the adsorption kinetics of the contaminants onto the TLP. Such studies are done to determine how fast the adsorption process takes place and to evaluate which model fits better according to the results obtained. Adsorption kinetics were determined based on the pseudo-first and pseudo-second-order kinetic models. The adsorption experiments were performed at constant temperature (25 °C), contaminant concentration (20 mg/L), and adsorbent dosage, while varying the contact time at 5, 15, 30, 60, 90, and 120 min. The pseudo-first-order model can be presented as given in Equation 7:

$$log\,(q_e - q_t) = \log(q_e) - \frac{k_1 t}{2.303} \tag{7}$$

Plotting log (q_e-q_t) versus time t gives a linear relationship with a slope corresponding to -k_1/2.303, and the intercept represents log (q_e). For pseudo-second order (Equation 8), plotting t/q_t against t yields a linear plot whose slope is 1/q_e and intercept of 1/$k_2q_e^2$ (Xu et al., 2022).

$$\frac{t}{q_t} = \left(\frac{1}{q_e}\right)t + \frac{1}{k_2 q_e^2} \tag{8}$$

In Equations 7, 8, q_e is the mass of contaminant adsorbed at equilibrium (mg/g), q_t is the mass of the contaminant adsorbed at time t (mg/g), k_1 is the pseudo-first order rate constant (min^{-1}), and k_2 is the pseudo-second order constant (g/mg/min).

The Elovich kinetic model was also used. The Elovich equation is applicable to chemical adsorption processes and is well-suited for systems with energetically non-uniform surfaces. At low surface coverage, interactions among the adsorbed species have a minimal influence on the adsorption kinetics. Moreover, as surface coverage increases, the adsorption energy rises linearly (Largitte and Pasquier, 2016). The parameters α and β represent the initial adsorption rate and the overall extent of adsorption, respectively, with β also serving as an indicator of the chemisorption mechanism. The linear equation used is given in Equation 9:

$$qt = 1\beta ln(\alpha\beta) + 1\,\beta\, lnt \quad (9)$$

In this equation, α is the initial adsorption rate (mg g^{-1} min^{-1}), and β is the desorption constant related to the extent of surface coverage and activation energy for chemisorption (g mg^{-1}). They can be calculated from the slope and intercept of the linear plot of q_t vs. ln(t).

2.7 Desorption experiment

Desorption was done to remove the adsorbed contaminants and assess the regeneration of the TLP. It was done as mentioned by Silva et al. (2021) with slight modifications. It was tested for crystal violet, where dye loaded biosorbent were desorbed using 50 mL of ethanol as the desorption solvent, and stirred at 120 rpm for 1 h. Then, they were filtered and washed with distilled water, dried, then tested for adsorption over three cycles.

2.8 Statistical analysis

IBM SPSS 27 software (SPSS Inc., Chicago, United States) was used for statistical analysis to assess the effectiveness of TLP in contaminant removal. One-way analysis of variance (ANOVA) test was applied at 99% confidence interval ($p < 0.01$). LSD test was applied to compare the means of each parameter within the same group of contaminants. Results were tested in triplicates and the presented results in the graphs are the mean ± standard deviation (mean ± sd).

3 Results and discussion

3.1 Infrared spectroscopic analysis

Infrared spectroscopy is a helpful technique for the determination of functional groups present in the sample studied. Figure 1a shows the Fourier Transform Infrared (FTIR) spectra of tomato leaves powder (TLP) before and after adsorption with the different contaminants at an initial concentration of 20 mg/L and contact time 30 min. Spectral analysis revealed significant shifts and changes in peak intensities, suggesting functional group interactions with the contaminant in the adsorption process. The major absorption band observed in the spectrum of untreated TLP sample was registered at 3420 cm^{-1} corresponding to O-H stretching vibrations of alcohols, phenols and/or carboxylic acids, which can be present in cellulose, hemicellulose, or lignin. These functional groups facilitate strong attractive interactions through hydrogen bonding between hydrogen bond donors and acceptors present in the contaminant (Pang et al., 2019). The lower intensity for CV and MB at this region suggests strong interactions between their molecules and hydroxyl groups through hydrogen bonding, reducing the availability of free O–H groups. In contrast, MG and lead showed higher intensities in this region, indicating less extensive interaction with O–H groups. The peak at 2910 cm^{-1} was attributed to the stretching vibration of C-H bond found in methyl group (Akanda et al., 2024). This region showed small changes after adsorption of CV, MB, and lead, while no significant change was observed upon adsorption of MG. The presence of characteristic carbonyl C=O was inferred from the stretching vibration at 1740 cm^{-1} in the untreated TLP, normally associated with lignin or hemicellulose (Akanda et al., 2024). This absorption band shifted to lower frequency (~1710 cm^{-1}) when the adsorbent encountered the contaminants, suggesting the weakening of the C=O bond and signifying the interaction between the carbonyl group and the pollutants. The absorption band at 1600 cm^{-1} was indexed to C=C of alkenes and aromatic functional groups. This band experienced changes in intensity upon interaction with the pollutants associated with slight shifts in the absorption frequency after MG adsorption, and more prominent shifts post lead adsorption. This can be attributed to the cation-π interactions between the positively charged lead ions or dyes and the aromatic systems in the adsorbent. Additionally, the peak at 1045 cm^{-1}, corresponding to C-O stretching vibration in cellulose and hemicellulose (Lupoi et al., 2015), showed decreased intensity post-adsorption with shifts in the absorption frequency, suggesting interaction through C-O groups with the contaminants. Small shifts, as observed after MG adsorption at 1600 cm^{-1}, or only peak intensity changes without shifts as seen for the rest of the dyes, suggested that the biosorption could occur through physical interaction (physisorption) or ion-exchange mechanisms. However, larger shifts, as observed with lead at the same wavenumber, could indicate that adsorption might be facilitated by complexation with the functional groups on TLP (Blázquez et al., 2011). Figure 1b presents the FTIR spectra of the free contaminants (CV, MB, MG, and Pb), serving as a comparative baseline to identify the characteristic vibrational bands of each contaminant. This allows for a clearer distinction between the original bands of the TLP and those introduced or affected by the adsorbed contaminant. By comparing Figures 1a,b, similar peaks with changes in peak intensities and some shifts after adsorption were reported. For example, the O-H stretching band at 3420 cm^{-1} clearly shows a change in intensity either forming a broader band or change in shape after adsorption. These comparative changes support the conclusion that adsorption has taken place and was facilitated by the identified functional groups on TLP. Tomato waste, including peel and seeds, were previously studied for the adsorption of pharmaceuticals from water (Pavlović et al., 2021). It is important to compare the functional groups present in both the waste and the leaf material to check for similarities in adsorption processes. Our results revealed functional groups consistent with those found in tomato waste including that both materials exhibited prominent hydroxyl (O-H), carbonyl (C=O), aromatic (C=C), and polysaccharide (C-O) bands, which are central to the biosorption process, confirming the presence of shared chemically active sites that facilitate adsorption. These findings validated the relevance of tomato leaf biomass as a functionally similar yet distinct adsorbent within the tomato waste spectrum.

3.2 X-ray diffraction analysis

The crystalline nature of TLP before and after adsorption was examined using XRD and the results are presented in Figure 2. Analyzing the XRD diffractogram of the untreated TLP suggested

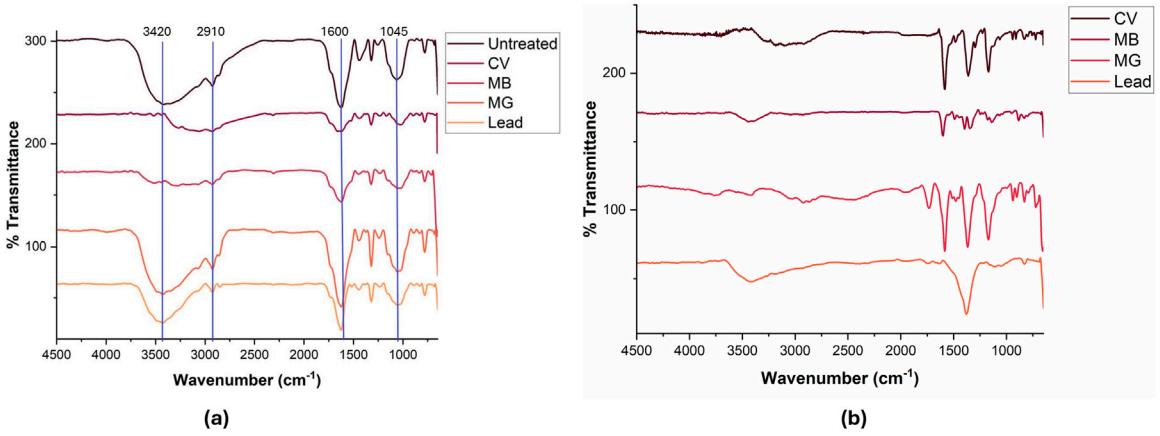

FIGURE 1
(a) FTIR spectra of TLP before and after the adsorption process with the contaminants. Concentration = 20 mg/L; time = 30 min; dosages: methylene blue (MB) 0.4 g; malachite green (MG): 0.6 g, crystal violet (CV): 0.2 g, lead: 0.9 g; agitation = 120 rpm, temperature = 25°C. **(b)**: FTIR spectra of contaminants: crystal violet (CV), methylene blue (MB), malachite green (MG), and lead nitrate.

that the general structure of the untreated TLP is amorphous with some minor crystalline phases, as inferred by the low intensity peaks. Peaks registered at 15.7°, 22.5°, and 34.5°, correspond to the crystalline regions of cellulose I, a primary structural component of plant cell walls. In contrast, the broad and weak peaks between 20° and 25° are characteristic of amorphous phases associated with lignin and hemicellulose, which are less structured compared to cellulose (Choi et al., 2018; Ma et al., 2019). A higher lignin and hemicellulose content in the material infers more amorphous and less crystalline structure (Renu et al., 2017). Amorphous surfaces are generally better suited than crystalline ones for the adsorption of multipollutants with different shapes and sizes (Kumar et al., 2014; Dey et al., 2022). Adsorption of the pollutants to the TLP matrix induced significant changes in the XRD pattern of the TLP-pollutant complex, suggesting a disruption in the original structure, and signifying adsorption activity. Prominent sharp peaks appeared, especially in the case of lead, indicating molecular alignment or ordered deposition of the contaminant onto TLP. These results corroborated the FTIR results that suggested significant interaction of TLP-functional groups with the contaminants. In addition, the fact that sharper peaks appeared after the interaction of TLP and the contaminants implied enhancement in the crystallinity of the adsorbent. Such observation was further supported by the findings of the SEM micrographs that also showed better crystallinity as will be discussed below. The combination of FTIR and XRD analyses suggested a multi-faceted adsorption mechanism that can indicate physisorption and ion exchange for cationic dyes, electrostatic interactions with surface complexations for lead, as well as hydrogen bonding and cation–π interactions mediated by the aromatic and polar functional groups present in the tomato leaf powder.

3.3 Scanning electron microscopy analysis

The morphology of TLP, before and after contaminant adsorption, was monitored by SEM and the collected micrographs are shown in Figure 3. The untreated biosorbent exhibited rough, irregular and porous structure with visible fibrillar and granular structures, indicative of a material that is well-suited for adsorption due to its numerous active sites (Khadim et al., 2022). After adsorption, many morphological changes were apparent. Lead adsorption resulted in the formation of dense crystalline deposits on the surface, with the pores and crevices largely filled. Similar results were recorded for the adsorption of lead onto cucumber peels, where surface modification was associated with the presence of micro particles of lead on the adsorbent surface (Basu et al., 2017). MB adsorption led to a smooth and uniform film-like coating over the surface, suggesting strong surface interactions and pore utilization. CV showed a more organized surface layer, with partially crystalline formations and pores almost fully blocked, indicating effective adsorption. As for MG, compact surface coverage and disappearance of ridges and pores implied uniform amorphous dye deposition. These results demonstrated the adaptability of TLP in capturing a variety of contaminants through structural modifications and surface coverage. Similar results were obtained with the use of bilberry leaves, where the heterogeneous surface with pores and folds present pre-adsorption became more homogenous and compact after MB adsorption indicating that the dye molecules filled up those pores (Mosoarca et al., 2022).

3.4 Effect of adsorbent dosage

To determine the minimum dosage required for the maximal adsorption of the contaminant, the adsorbent dosages were tested in a range from 0.1 g/100 mL to 0.9 g/100 mL. The contaminant solution was set at a concentration of 20 mg/L throughout the experiments. Figure 4 shows the results for the adsorption of the different contaminants: MB, MG, CV, and lead. The adsorption capacity of methylene blue increased from 88.6% ± 0.17 at 0.1 g of adsorbent to a maximum of 90.6% ± 0.3 at 0.4 g of adsorbent. Further increase in the amount of adsorbent did not improve the percentage of MB removal from the solution which decreased at a higher dosage of TLP. For malachite green, the highest adsorption

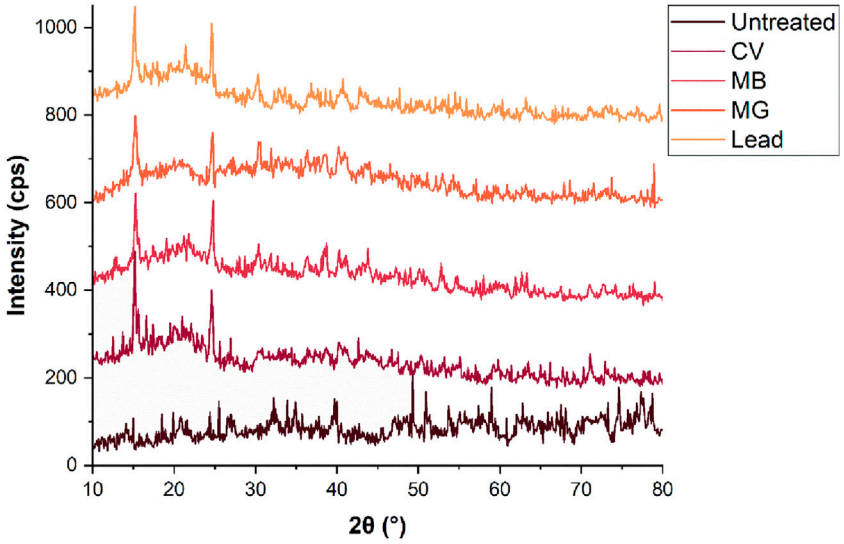

FIGURE 2
XRD of TLP before and after the adsorption of the contaminants. Concentration = 20 mg/L; time = 30 min; dosages: methylene blue (MB) 0.4 g; malachite green (MG): 0.6 g, crystal violet (CV): 0.2 g, lead: 0.9 g; agitation = 120 rpm, temperature = 25°C.

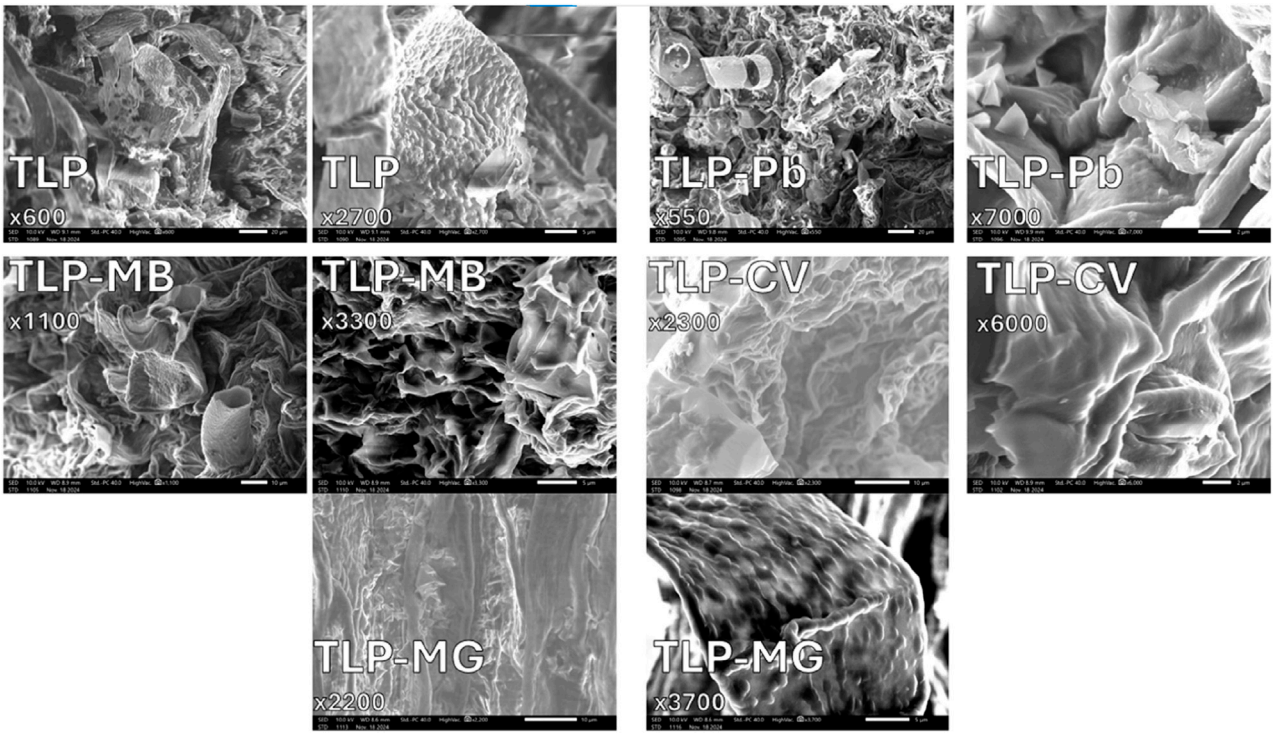

FIGURE 3
SEM images of TLP before and after the adsorption of the contaminants under investigation. Concentration = 20 mg/L; time = 30 min; dosages: methylene blue (MB) 0.4 g; malachite green (MG): 0.6 g, crystal violet (CV): 0.2 g, lead: 0.9 g; agitation = 120 rpm, temperature = 25°C.

capacity of 93.63% ± 0.2 was achieved at 0.6 g/100 mL, up from 77.3% ± 0.1 at 0.1 g. In the case of crystal violet, the maximum adsorption capacity of 89.71% ± 0.2 occurred at 0.2 g, increasing from 87.5% ± 0.3 at 0.1 g. A study using an unmodified leaf biosorbent, specifically *Tabernaemontana divaricata*, tested the efficiency of the leaf powder in removing crystal violet and reported that 4 g/L was the dose of choice to achieve removal percentage similar to the ones achieved at 2 g/L in the current study (Akanda et al., 2024). This shows that TLP achieves comparable adsorption efficiency at a significantly lower dose, highlighting its

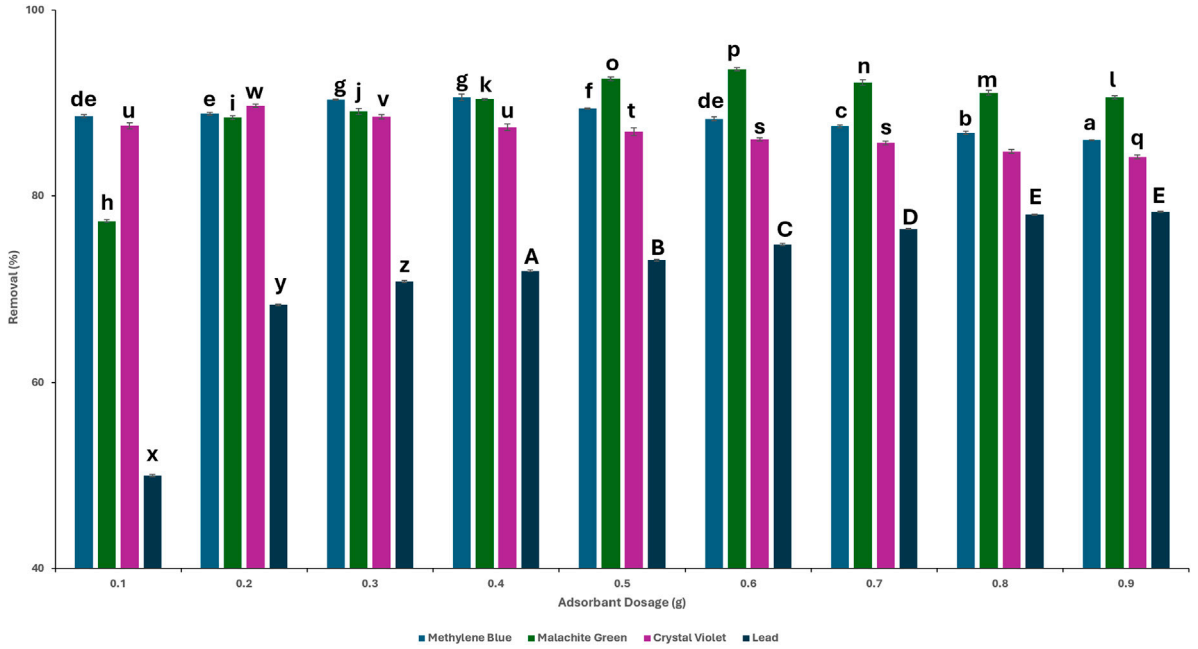

FIGURE 4
Removal percentages of the contaminants at different initial TLP dosages. Concentration = 20 mg/L; time = 120 min; agitation = 120 rpm, temperature = 25°C. LSD test performed between contaminant groups. Different letters above bars indicate statistically significant differences ($p < 0.01$).

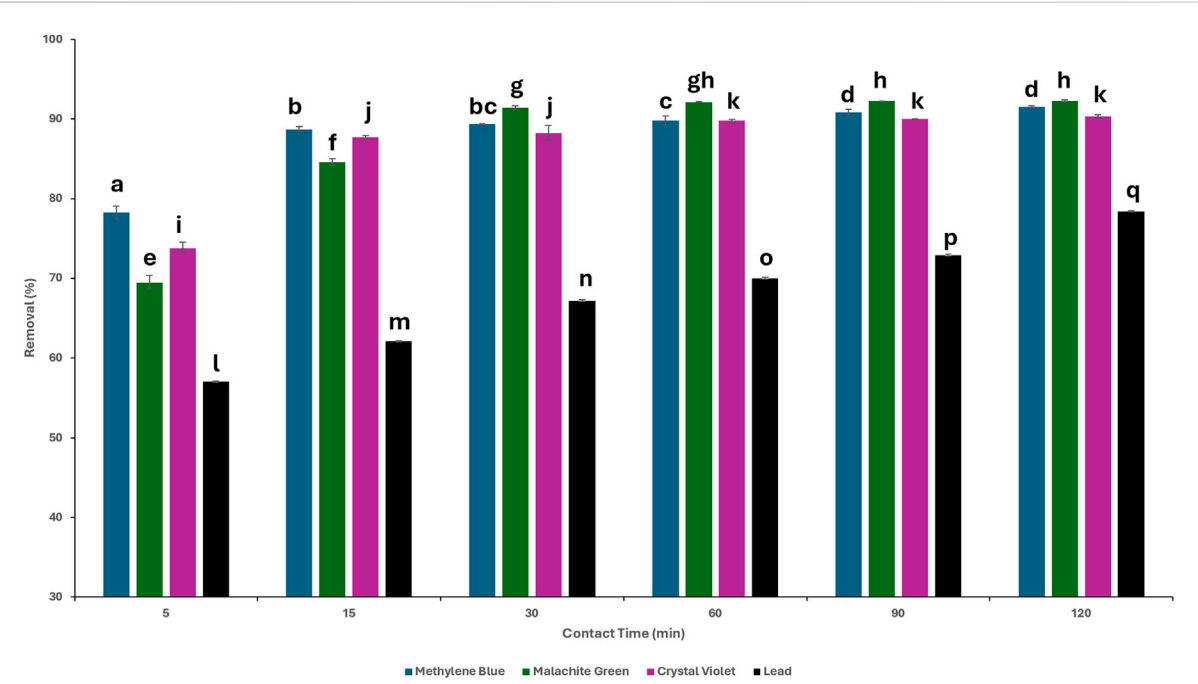

FIGURE 5
Removal percentages of the contaminants at different times. Concentration = 20 mg/L; dosages: methylene blue (MB) 0.4 g; malachite green (MG): 0.6 g, crystal violet (CV): 0.2 g, lead: 0.9 g; agitation = 120 rpm, temperature = 25°C. LSD test performed between contaminant groups. Different letters above bars indicate statistically significant differences ($p < 0.01$).

superior adsorption capacity and potential cost-effectiveness when removing CV. On the other hand, the percentage of lead removal increased concomitantly with the amount of adsorbent used where a maximum adsorption capacity of 78.4% ± 0.1 was attained at 0.9 g of TLP, with a steady state beginning to appear at 0.8 g (78% ± 0.1). These results demonstrated that increasing the number of

biosorbent particles enhances adsorption by providing a larger surface area for contaminant attachment. Beyond a certain threshold, an increase in biosorbent dosage did not improve adsorption efficiency as evidenced by either stabilization or decline in adsorption after the optimal removal was attained. This suggested that after a saturation point is reached, more TLP no longer contributed to improved contaminant removal (Fu et al., 2021). The one-way ANOVA test showed a significant relationship ($p < 0.01$) between different TLP dosages and the removal percentage of the contaminants. For MB, a significant statistical difference between 0.4 g/100 mL and 0.5 g/100 mL was observed since there was a slight decrease after 0.4 g/100 mL, indicating 0.4 g as the better dosage to use. For MG and CV, it was at 0.6 g and 0.2 g, respectively, as there was a significant decrease in the removal percentage after these values. For lead, equilibrium was reached at 0.9 g/100 mL. The adsorbent dosages chosen for the rest of the study were 0.4 g for MB, 0.6 g for MG, 0.2 g for CV, and 0.9 g for lead.

3.5 Effect of contact time on adsorption

One of the crucial parameters influencing the process of adsorption is the contact time between the adsorbent and adsorbate (Manzoor et al., 2019). This effect was tested at 5, 15, 30, 60, 90, and 120 min, while keeping the TLP dosage and contaminant concentration constant. Figure 5 shows the effect of contact time on contaminant adsorption. For the adsorption of MB, a rapid uptake was shown during the first 5 min with 78.2% adsorption, reaching 91.5% at 120 min. MG displayed an initial adsorption of 69.5% in the first 5 min, increasing to 92.3% at 120 min. As for CV, it showcased a 73.8% adsorption within the first 5 min to reach 90.3% at 120 min. For the lead solution, 57.1% adsorption was achieved during the first 5 min, reaching 78.4% at 120 min. One-way ANOVA revealed that there was a statistically significant relationship ($p < 0.01$) between the removal percentages of contaminants and increase in contact time. In specific, the percentage of dye removal increased concomitantly with contact time up to a certain point. Beyond this point, there was no statistically significant enhancement in removal, indicating that equilibrium has been attained. In the case of MB, equilibrium was achieved at 90 min as there was no statistically significant difference in % removal after that time point. For MG and CV, equilibrium was reached at 30 min, while for lead, % removal remained significant throughout the 120 min. The particle vacant sites allow for rapid binding of the contaminant leading to fast adsorption. However, reduced site availability slows down the biosorption process, leading to equilibrium and indicating the maximum capacity of adsorption (Sen, 2023).

3.6 Effect of initial contaminant concentration on adsorption

The effect of the initial contaminant concentration on the adsorption capability of TLP was determined by varying the initial concentration of each contaminant, while keeping the previously set parameters constant consisting of an initial TLP dosage of 0.4 g for MB, 0.2 g for CV, 0.6 g for MG, and 0.9 g for lead with a contact time of 120 min. Figure 6 shows the results for

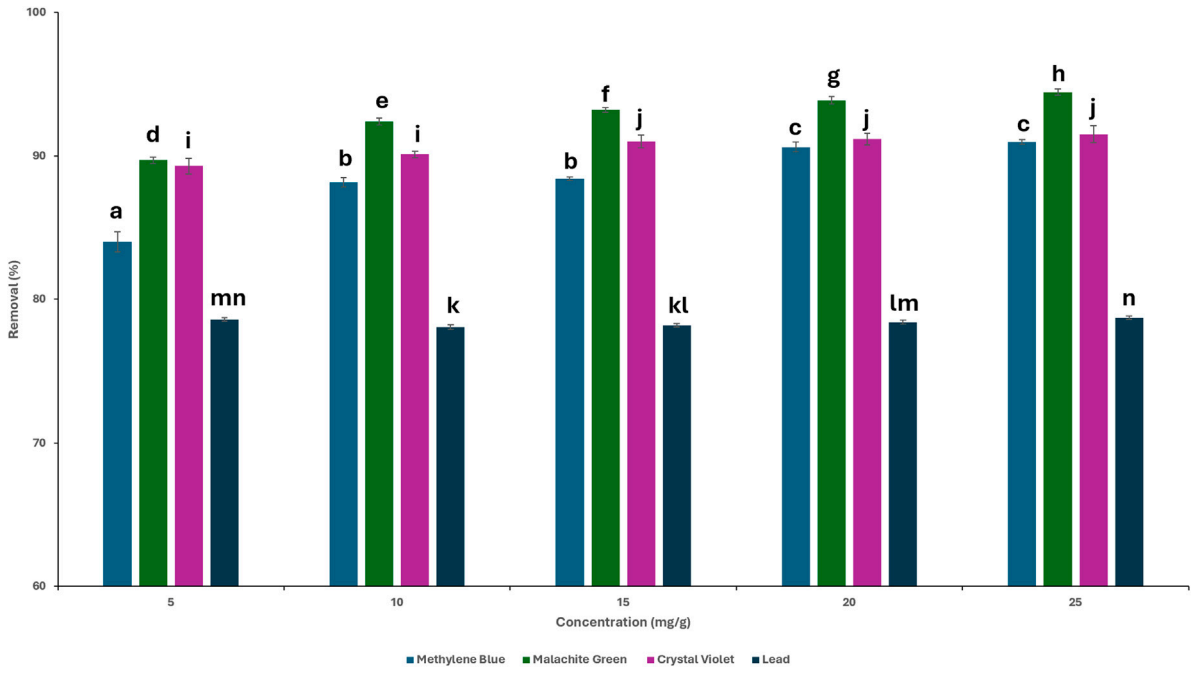

FIGURE 6
Removal percentages of the contaminants at different initial concentrations. Time = 120 min; dosages: methylene blue (MB) 0.4 g; malachite green (MG): 0.6 g, crystal violet (CV): 0.2 g, lead: 0.9 g; agitation = 120 rpm, temperature = 25°C. LSD test performed between contaminant groups. Different letters above bars indicate statistically significant differences ($p < 0.01$).

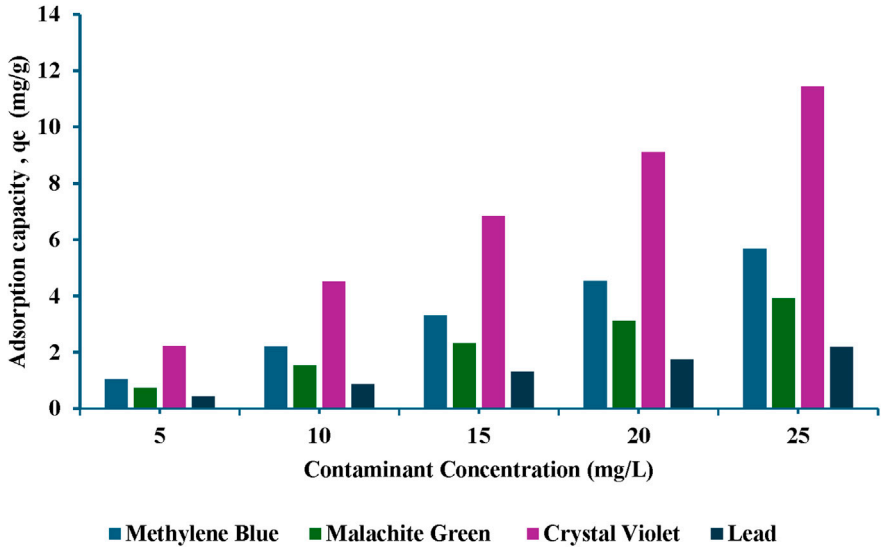

FIGURE 7
Removal efficiency of contaminants at different initial concentrations. Time = 120 min; dosages: methylene blue (MB) 0.4 g; malachite green (MG): 0.6 g, crystal violet (CV): 0.2 g, lead: 0.9 g; agitation = 120 rpm, temperature = 25°C.

each contaminant at the different concentrations, specifically at 5, 10, 15, 20 and 25 mg/L. It can be noted that as the concentration of the dyes increased, the removal percentage increased. However, above a certain concentration level, the removal percentage became constant. This was most likely due to the increase in the number of dye molecules available for adsorption while the adsorbent amount stayed the same. As the concentration of the dyes increased, a greater number of binding sites on the adsorbent were filled, leading to enhanced adsorption capabilities (Zhang et al., 2019). One-way ANOVA showed that there was a significant relationship ($p < 0.01$) between the removal percentages and the initial dye contaminant concentration. For MB, there was no statistically significant difference observed between 20 and 25 mg/L, indicating equilibrium was reached at this concentration range. For MG, the removal percentage remained statistically significant throughout the tested concentrations. For CV, equilibrium was reached at 15 mg/mL as no significant difference was observed after this concentration. In the case of lead, there was no statistical significance across 5–25 mg/L, with minor statistical difference between 5 and 10 mg/L, indicating that the removal % was stable, and suggesting that the adsorption process was effective and stable irrespective of the initial concentration of the solution. Adsorption capacity of the adsorbent was evaluated at different concentrations of the contaminants, and results were expressed as the amount adsorbed per gram of adsorbent, q_t (mg/g), as shown in Figure 7. It has been demonstrated that increasing the concentration of the contaminant enhanced the adsorption capacity of the biosorbent. The increase in adsorption capacity is due to the high initial concentration, which acts as a driving force to promote mass transfer (Chouchane et al., 2023). TLP was analyzed for lead content to assess the potential contamination tendency of the biosorbent. Surprisingly, the raw TLP powder contained 2.2 mg/kg of lead. Despite the presence of lead in the sample, TLP still showed high adsorption efficiency as inferred from the reported results. These findings underscore the utility of TLP as natural biosorbent. Instead of disposing the lead-contaminated tomato leaves into the environment where natural degradation processes can facilitate the leaching of lead into the soil and other natural resources, TLP was utilized for the biosorption of heavy metals. The valorization of agricultural waste as described in this report offered the means for hazardous pollutants removal while simultaneously mitigating environmental pollution. Moreover, the spent powder could be repurposed into several potential applications to align with the principles of circular economy. These include, among others, using it as natural filler in brick composites. In addition, bacterial remediation to remove heavy metals from the powder could explored in future studies., The use of unmodified TLP was favored in this study due to its low-cost, energy-free preparation which showcased an effective adsorption performance, making it suitable for scalable and sustainable applications.

3.7 Adsorption isotherms

The experimental data were fitted to the Langmuir and Freundlich adsorption isotherm models to better understand the mechanism of adsorption by TLP for each of the contaminants. Adsorption isotherms provide insight into the interaction between the adsorbate and the adsorbent at equilibrium. In other words, it relates the solute concentration on an adsorbent surface to its equilibrium concentration in the liquid with which it is in contact. These relationships are essential to better understand the fundamental mechanisms of adsorption as well as the surface properties of adsorbate and adsorbent. Different models are applied in adsorption studies with the most common ones being the Langmuir and Freundlich isotherms. The Langmuir model is based on the assumption of a monolayer adsorption on a

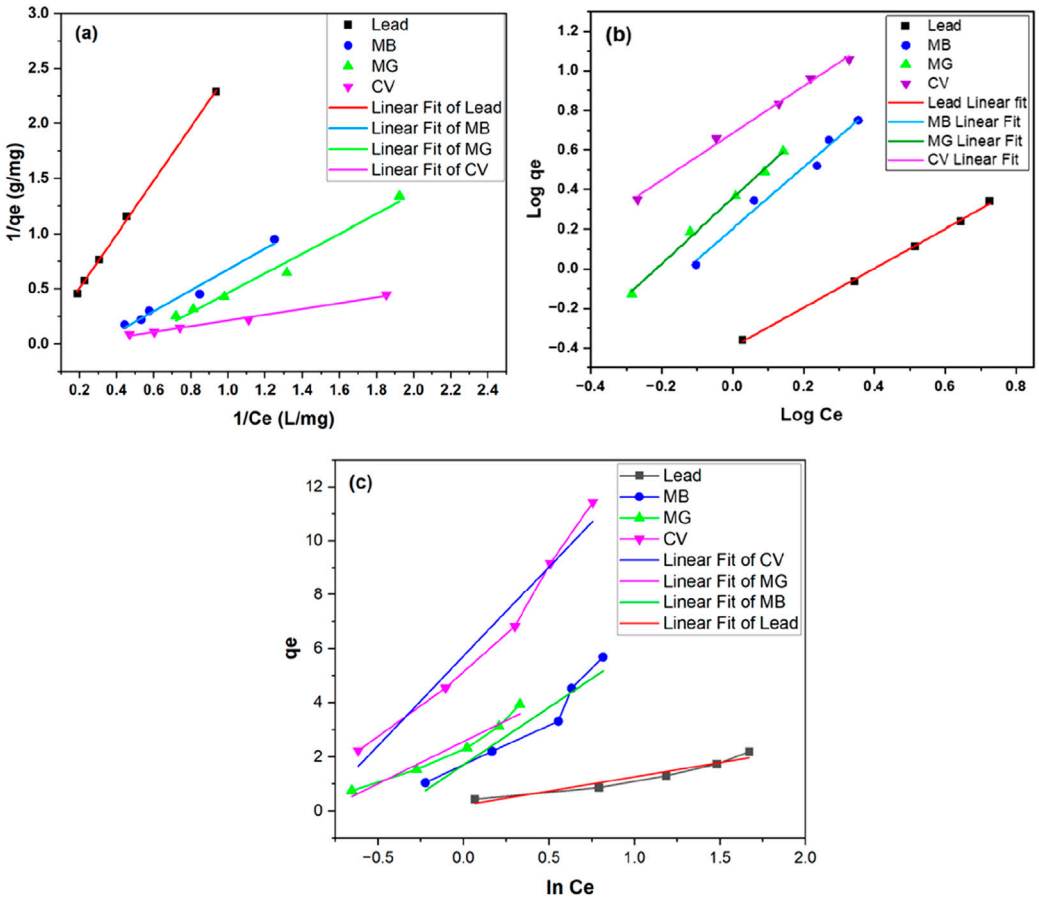

FIGURE 8
Adsorption isotherm: **(a)** Langmuir, **(b)** Freundlich, **(c)** Temkin.

TABLE 1 Langmuir, Freundlich, and Temkin isotherm model parameters. (MB: Methylene Blue, MG: Malachite green, CV: Crystal violet).

	Langmuir				Freundlich			Temkin			
	q_m (mg/g)	K_L (L/mg)	R_L	R^2	K_F (mg/g)	n	R^2	KT (L/g)	b (J/mol)	b (Kcal/mol)	R^2
Lead	45.77	0.00898	0.884	0.99904	0.402	1.0037	0.99882	1.231	23,966.6	5.73	0.9096
MB	−3.67	−0.2864	−2.319	0.97644	1.552	0.6292	0.98401	1.495	583.54	0.14	0.9042
MG	−2.32	−0.4812	−0.711	0.98144	2.275	0.6046	0.99664	2.285	797.51	0.19	0.9390
CV	−20.64	−0.1845	12.948	0.99038	4.842	0.8390	0.9947	2.375	374.29	0.09	0.9534

homogenous adsorption surface with strong interactions between adsorbate and adsorbent. It also states that the adsorption takes place at exclusive specific active sites, with each site holding a single molecule independently, without any interactions between the adsorbed molecules or changes in the physical state (Al-Saeedi et al., 2023). In contrast, the Freundlich isotherm model suggests that the adsorption surface can improve itself, allowing for heterogeneous adsorption, through multi-layer surface interaction. If the Langmuir isotherm effectively explains the adsorption data, the process is most likely to be chemisorption since it indicates unimolecular adsorption. However, if the data better fits the Freundlich isotherm, then the mechanism is more likely considered to be physisorption with the multilayer adsorption (Mate and Mishra, 2020; Alafnan et al., 2021). Temkin isotherm was also tested. The graphical representation of Langmuir, Freundlich, and Temkin isotherms are presented in Figures 8a–c, respectively. The parameters obtained for the equations of the isotherms are presented in Table 1.

The coefficients of determination (R^2) for each isotherm were used to assess the fit of the experimental data to the isotherm (Piepho, 2019). The adsorption of lead onto TLP was described effectively by both Langmuir and Freundlich isotherm models, as demonstrated by the high R^2 for each model with 0.99882 for Freundlich and 0.99904 for Langmuir, indicating an excellent fit to both isotherms.

TABLE 2 Comparison of maximum adsorption capacity (qm) of tomato leaves powder with other unmodified biosorbents.

Adsorbent material	Maximum adsorption capacity (mg/g)	References
Tomato leaves	45.77	Present study
Banana peels	2.18	Anwar et al. (2010)
Tea waste	33.49	Wan et al. (2014)
Walnut shell	9.912	Çelebi and Gök (2017)
Spent coffee ground	48.13	Futalan et al. (2019)
Azadirachta indica (neem) Leaves	39.7	Elkhaleefa et al. (2021)
Moringa oleifera leaves	14.124	Imran et al. (2019)

However, Langmuir is considered the better fit due to the slightly higher R^2 making it of choice for explaining the adsorption mechanism. This model suggests that the adsorption process occurs at specific homogenous sites on the adsorbent surface, forming a monolayer of lead ions without stacking or forming multilayers. The maximum adsorption capacity (q_m) represents the maximum amount of lead ions that can be adsorbed per gram of TLP under the tested conditions. In the current study, qm had a value of 45.77 mg/g, suggesting that TLP exhibited a high capacity for lead removal. This maximum adsorption capacity is higher than the one achieved by other leaf adsorbates such as *Azadirachta indica* (neem leaves), which showed a maximum adsorption capacity of 39.7 mg/g for lead (Elkhaleefa et al., 2021). It is also comparable to modified biosorbents such as activated carbon derived from sawdust that was used to adsorb methyl orange with a maximum adsorption capacity close to 1.78 mg/g (Sultana et al., 2024). Table 2 compares the q_m with other studies that used unmodified biomass as their adsorbate. The Langmuir constant K_L, related to the affinity between the TLP adsorbent and lead ions, had a value of 0.00898 L/mg, showing a moderate affinity between lead ions and TLP. As for the separation factor, R_L, all values were between 0 and 1, with an average of 0.884, indicating that adsorption is favorable. In a study involving the adsorption of lead onto olive tree pruning waste, both Langmuir and Freundlich isotherms had high R^2 values of 0.993 and 0.986, respectively, suggesting that multiple adsorption mechanisms may be happening, and that some heterogeneity may exist in the adsorption sites on the adsorbent surface (Blázquez et al., 2011). The value of the adsorption intensity (n), for lead is close to 1, indicating that the adsorption is linear. The experimental data was also fitted into the Henry isotherm which assumes that the amount of the adsorbate (q_e) is linearly proportional to its concentration in the solution (C_e) (Kalam et al., 2021). Interestingly, a linear graph with R^2 close to unity was generated when q_e was plotted against C_e demonstrating the goodness of fit into the studied model (Figure 9). Nevertheless, the Henry model can be best applied at low concentrations of the adsorbate as it assumes that molecules interact independently with a homogenous surface whose active sites are identical.

The Freundlich isotherm provided the better fit for all dye-treated TLP according to the value of R^2, as depicted in Table 1. This indicates that dye adsorption occurred on a heterogeneous surface in a multilayer manner. For MB, the value of n was 0.6292 ($0 < n < 1$), indicating a favorable adsorption process. Similar results were obtained for MG and CV with the values of n being 0.6046 and

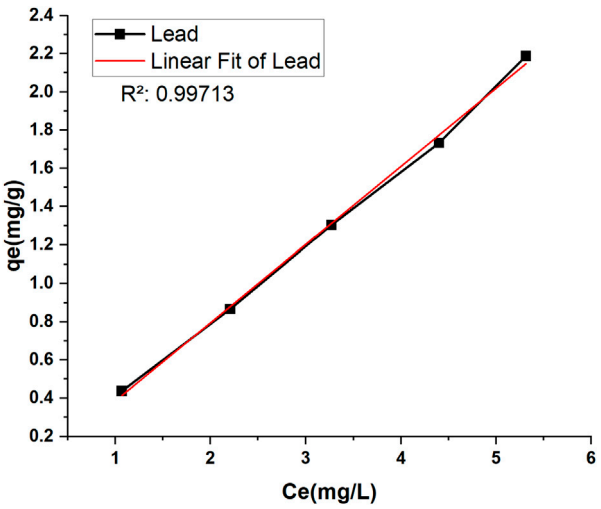

FIGURE 9
Henry Adsorption Isotherm applied to lead-treated tomato leaf powder.

0.8390, respectively. This implied that the adsorption of all tested dyes on TLP was favorable. The negative values seen in Langmuir results for dyes indicate that the Langmuir adsorption isotherm was not suitable to explain the adsorption mechanism. Similar results were reported when the effect of modified and unmodified maize cob was tested for the adsorption of Cd (II), Pb (II), and Zn (II) at two particle sizes (Igwe and Abia, 2007). Negative values were seen for modified maize cob, indicating that Langmuir was not the good fit in this case.

While the Temkin isotherm demonstrated a good fit for the experimental data (R^2 between 0.909 and 0.953), the Langmuir and Freundlich isotherms were still the better choice for lead and dyes, respectively. The b value can infer the type of the sorption process (physisorption or chemisorption). Values less than 1 kcal/mol indicate physisorption, values between 1 and 20 kcal/mol suggest a combination of physical and chemical adsorption, and values between 20 and 50 kcal/mol are characteristic of chemisorption (Ettish et al., 2021). As can be seen in Table 1, for dyes, b ranged between 0.09 and 0.15 kcal/mol indicating physisorption mechanism that aligns with Freundlich isotherm. As for lead, the value of b was

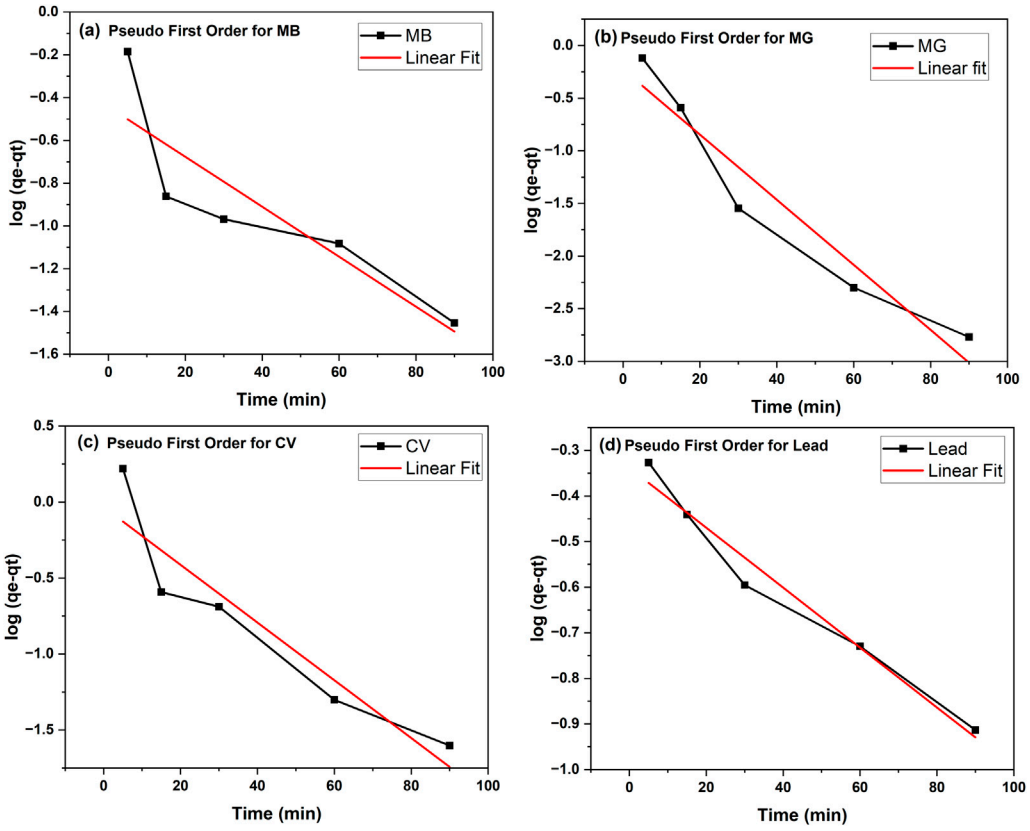

FIGURE 10
Kinetic studies on the adsorption of contaminants onto tomato leaf powder fitted to the pseudo-first order model. **(a)** Pesudo first order for MB **(b)** Pesudo first order for MG **(c)** Pesudo first order for CV **(d)** Pesudo first order for lead.

5.73 kcal/mol, suggesting a combination of physical and chemical adsorption in agreement with its good fit to both Langmuir and Freundlich isotherms.

The surface of the tomato leaves is rich in carboxyl groups, as indicated by the FTIR spectrum, which enhances electrostatic interactions between the adsorbent and cationic dyes, as well as the positively charged lead ions (Chen et al., 2021). Initially, attractive forces will dominate, facilitating adsorption, particularly when active sites on the surface are available. However, as these sites become occupied, repulsive forces may begin to emerge, potentially influencing the maximum adsorption capacity. While electrostatic interactions play a crucial role in the effective removal of contaminants, they are not the only forces at play. Other interactions, such as hydrogen bonding (between hydrogen bond donors like OH, NH, and SH groups, and acceptors like O, N, S, and halogens), as well as dipole-dipole and ion-dipole interactions, further contribute to the adsorption process (Radwan et al., 2023).

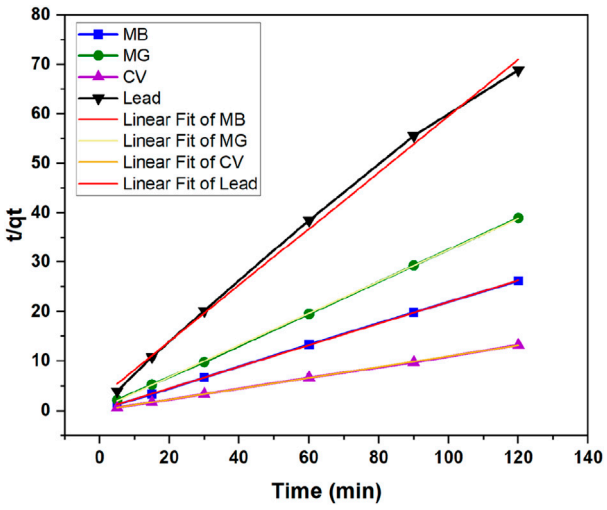

FIGURE 11
Kinetic studies on the adsorption of the contaminants onto tomato leaf powder using the pseudo-second order model.

3.8 Kinetic studies

To monitor the kinetics of the adsorption process and possibly assess its mechanism, the results from the adsorption studies at different contact times were analyzed by fitting the data to the pseudo-first order or pseudo-second order models. The graphical representations of adsorption data fitted to the pseudo-first- and pseudo-second-order equations are presented in Figures 10, 11,

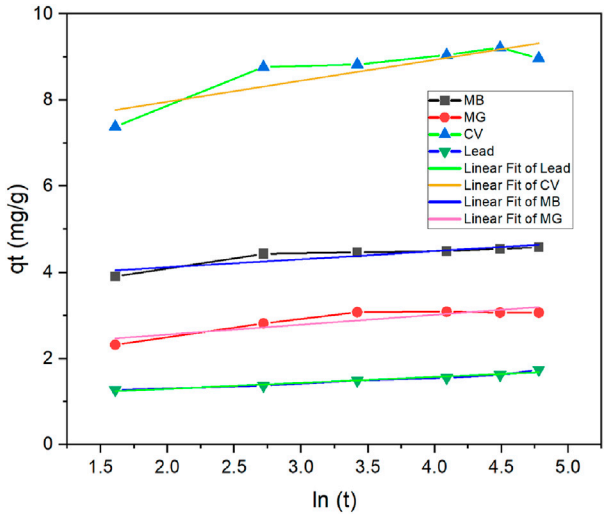

FIGURE 12
Kinetic studies on the adsorption of the contaminants onto TLP using the Elovich model.

respectively. The fitting parameters are summarized in Table 3 for all contaminants.

As can be seen in Table 3, the adsorption kinetics for all contaminants were best fitted to the pseudo-second order model, as the R^2 of all samples was >0.99. On the other hand, R^2 values ranged between 0.7716 and 0.9727 when data was fitted into the pseudo-first order model. The values of the calculated q_e from pseudo-second order model were in line with the experimental results, further indicating that the pseudo-second order is a better fit model. For example, in the case of lead, the calculated q_e obtained was 1.573 mg/g, which is very close to the experimental value (1.742). The pseudo-second order kinetics suggests that the adsorption rate depends more on the adsorption capacity and consequently the number of active sites, rather than on the adsorbate concentration (Fito et al., 2023). Elovich model was also conducted with graphical presentations shown in Figure 12 with parameters α and β displayed in Table 3. The best fitted data was for lead with an R^2 of 0.954. This indicates that this model can be a good fit for explaining lead adsorption but pseudo-second order was still the better fit. However, the results of this model further confirm that the sorption tends to be more chemisorption where the interaction between the biosorbent and adsorbate occurs by a chemical bond (Aguiar et al., 2022). The results for the dyes do not show a good fit to this model with R^2 ranging between 0.768 and 0.806, as accompanied with unrealistically high values for α, indicating that sorption process is not chemisorption. All in all, pseudo-second order seems to be the better fit when choosing the kinetic model to best explain the results of the contaminants adsorption onto TLP.

TABLE 3 Pseudo-first and second order model parameters (MB: Methylene Blue, MG: Malachite Green, CV: Crystal Violet).

	Pseudo-first order			Pseudo-second order			Experimental q_e	Elovich model		
	R^2	K_1	q_e	R^2	K_2	q_e		α (mg/g·min)	β (g/mg)	R^2
Lead	0.9727	0.0152	0.460	0.9961	0.127	1.573	1.742	215.86	7.21	0.954
MB	0.7716	0.0269	0.360	0.9999	0.2487	4.599	4.53	149,000,000	5.46	0.797
MG	0.9322	0.0712	0.594	0.9999	0.2566	4.598	3.12	2,138.3	4.35	0.806
CV	0.8795	0.0438	0.926	0.9998	0.122	9.157	9.11	773,546.2	2.04	0.768

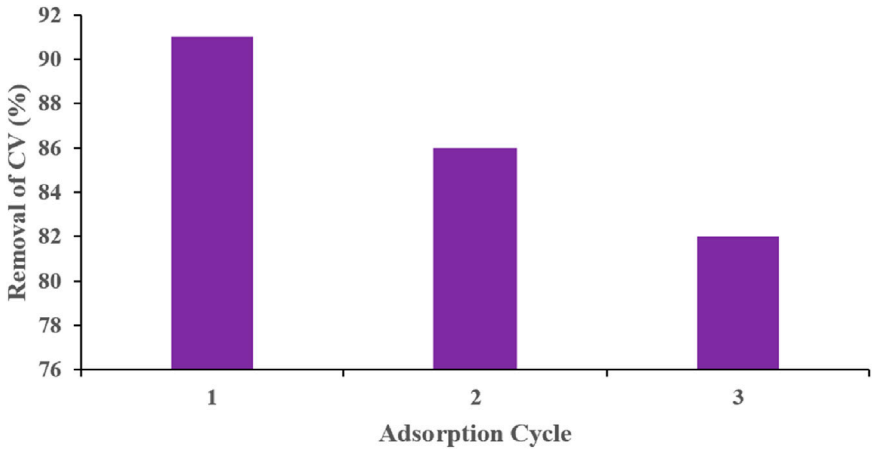

FIGURE 13
Regeneration of TLP with Crystal Violet (CV).

3.9 Recycling of the adsorbent

After a preliminary comparison between 70% and 90% ethanol revealed no significant difference in desorption performance, 70% ethanol was selected as the regeneration solvent. As shown in Figure 13, the regeneration efficiceny of TLP declined with repeated use reaching about 82% by the third cycle. The decrease in CV removal efficiency remained under 10% dropping from 91% in the first cycle to 82% by the third one. These results indicate that TLP possesses good regeneration capacity and can be effectively resused for multiple adsorption cycles.

4 Conclusion

This study shows the potential of tomato by-products, particularly leaves, as an effective, low-cost, and sustainable solution for purification of water from contaminants. The leaves demonstrated high adsorption capabilities for different dyes (methylene blue, malachite green, crystal violet) and for lead. Characterization by various techniques confirmed the functional groups and structural attributes that played a role in effective contaminant removal, while kinetic and isotherm studies shed light on the adsorption mechanisms. Pseudo-second-order kinetics fit the adsorption data of all contaminants. Lead was best fitted to the Langmuir isotherm while the dyes were best fitted to the Freundlich isotherm. These findings emphasize the potential of such agricultural by-products as an eco-friendly and cost-effective approach to solve the problem of water contamination, in particular industrial wastewater that contains these harmful chemical contaminants, while highlighting the requirement of future work to enhance efficiency and real-life application through field trials in diverse environmental and industrial scenarios.

Data availability statement

The raw data supporting the conclusions of this article will be made available by the authors, without undue reservation.

Author contributions

LH: Methodology, Data curation, Conceptualization, Writing – original draft. SS: Methodology, Writing – review and editing. AH: Writing – review and editing. MA: Writing – original draft, Data curation. HNR: Writing – review and editing. MAB: Writing – original draft, Data curation. MED: Writing – review and editing, Data analysis. NED: Conceptualization, Funding acquisition, Project administration, Validation, Writing – review and editing.

Funding

The author(s) declare that financial support was received for the research and/or publication of this article. This research was implemented with the support of the Arab-German Young Academy of Sciences and Humanities (AGYA); grant category as a Research Mobility Program (RMP). AGYA was funded by the German Federal Ministry of Education and Research (BMBF) grant 01DL20003.

Conflict of interest

The authors declare that the research was conducted in the absence of any commercial or financial relationships that could be construed as a potential conflict of interest.

Generative AI statement

The author(s) declare that no Generative AI was used in the creation of this manuscript.

Publisher's note

References

Aguiar, A. B. S., Costa, J. M., Santos, G. E., Sancinetti, G. P., and Rodriguez, R. P. (2022). Removal of metals by biomass derived adsorbent in its granular and powdered forms: adsorption capacity and kinetics analysis. *Sustain. Chem.* 3 (4), 535–550. doi:10.3390/suschem3040033

Ahmed, F., Ali, I., Kousar, S., and Ahmed, S. (2022). The environmental impact of industrialization and foreign direct investment: empirical evidence from Asia-Pacific region. *Environ. Sci. Pollut. Res. Int.* 29 (20), 29778–29792. doi:10.1007/s11356-021-17560-w

Akanda, M. R., Sohrawordi, M., Haque, M. A., Shahrear, M. S., and Ahmed, N. (2024). Preparation of novel green adsorbent (Tabernaemontana divaricata leaf powder) and evaluation of its dye (malachite green) removal capacity, mechanism, kinetics, and phytotoxicity. *S Afr. J. Chem. Eng.* 49, 178–188. doi:10.1016/j.sajce.2024.05.005

Alafnan, S., Awotunde, A., Glatz, G., Adjei, S., Alrumaih, I., and Gowida, A. (2021). Langmuir adsorption isotherm in unconventional resources: applicability and limitations. *J. Pet. Sci. Eng.* 207, 109172. doi:10.1016/j.petrol.2021.109172

Aljawrneh, B., Ocak, Y. S., Albiss, B. A., Dwiri, A., Tawalbeh, M., and Al-Othman, A. (2024). ZrO2 nanoparticles for effective dye degradation in wastewater: synthesis, characterization, and photocatalytic performance under sunlight. *J. Alloys Compd.* 15, 1008. doi:10.1016/j.jallcom.2024.176522

Al-Saeedi, S. I., Areej, A., Qamar, M. T., Alhujaily, A., Iqbal, S., Alotaibi, M. T., et al. (2023). Isotherm and kinetic studies for the adsorption of methylene blue onto a novel Mn3O4-Bi2O3 composite and their antifungal performance. *Front. Environ. Sci.* 11, 1156475. doi:10.3389/fenvs.2023.1156475

Anwar, J., Shafique, U., Waheed-uz-Zaman, Salman, M., Dar, A., and Anwar, S. (2010). Removal of Pb(II) and Cd(II) from water by adsorption on peels of banana. *Bioresour. Technol.* 101 (6), 1752–1755. doi:10.1016/j.biortech.2009.10.021

Arabkhani, P., and Asfaram, A. (2020). Development of a novel three-dimensional magnetic polymer aerogel as an efficient adsorbent for malachite green removal. *J. Hazard Mater* 384, 121394. doi:10.1016/j.jhazmat.2019.121394

Baby, R., Saifullah, B., and Hussein, M. Z. (2019). Palm kernel shell as an effective adsorbent for the treatment of heavy metal contaminated water. *Sci. Rep.* 9 (1), 18955–11. doi:10.1038/s41598-019-55099-6

Basic Information about Lead in Drinking Water (2025). US EPA. Available online at: https://www.epa.gov/ground-water-and-drinking-water/basic-information-about-lead-drinking-water

Basu, M., Guha, A. K., and Ray, L. (2017). Adsorption of lead on cucumber peel. *J. Clean. Prod.* 151, 603–615. doi:10.1016/j.jclepro.2017.03.028

Bizzi, C. A., Flores, E. M. M., Barin, J. S., Garcia, E. E., and Nóbrega, J. A. (2011). Understanding the process of microwave-assisted digestion combining diluted nitric acid and oxygen as auxiliary reagent. *Microchem. J.* 99 (2), 193–196. doi:10.1016/j.microc.2011.05.002

Blázquez, G., Martín-Lara, M. A., Tenorio, G., and Calero, M. (2011). Batch biosorption of lead(II) from aqueous solutions by olive tree pruning waste: equilibrium, kinetics and thermodynamic study. *Chem. Eng. J.* 168 (1), 170–177. doi:10.1016/j.cej.2010.12.059

Bolisetty, S., Peydayesh, M., and Mezzenga, R. (2019). Sustainable technologies for water purification from heavy metals: review and analysis. *Chem. Soc. Rev.* 48 (2), 463–487. doi:10.1039/c8cs00493e

Bourmaud, A., Konschak, K., Buffet, C., Calatraba, M., Rudolph, A. L., Kervoëlen, A., et al. (2023). A circular approach for the valorization of tomato By-Product in biodegradable injected materials for horticulture sector. *Polym. (Basel)* 15 (4), 820. doi:10.3390/polym15040820

Çelebi, H., and Gök, O. (2017). Evaluation of lead adsorption kinetics and isotherms from aqueous solution using natural walnut shell. *Int. J. Environ. Res.* 11 (1), 83–90. doi:10.1007/s41742-017-0009-3

Chen, K., Du, L., Gao, P., Zheng, J., Liu, Y., and Lin, H. (2021). Super and selective adsorption of cationic dyes onto carboxylate-modified passion fruit peel biosorbent. *Front. Chem.* 9, 646492. doi:10.3389/fchem.2021.646492

Choi, M., Kang, Y. R., Lim, I. S., and Chang, Y. H. (2018). Structural characterization of cellulose obtained from extraction wastes of graviola (Annona muricata) leaf. *Prev. Nutr. Food Sci.* 23 (2), 166–170. doi:10.3746/pnf.2018.23.2.166

Chouchane, T., Boukari, A., Khireddine, O., Chibani, S., and Chouchane, S. (2023). Equilibrium, kinetics, and thermodynamics of batch adsorption of Mn(II) ions on blast furnace slag (BFS) and kaolin (KGA). *J. Eng. Appl. Sci.* 70 (1), 58–20. doi:10.1186/s44147-023-00218-4

Deng, H., Zhang, J., Huang, R., Wang, W., Meng, M., Hu, L., et al. (2022). Adsorption of malachite green and Pb2+ by KMnO4-Modified biochar: insights and mechanisms. *Sustainability* 14 (4), 2040. doi:10.3390/su14042040

Dey, S., Sreenivasulu, A., Veerendra, G. T. N., Phani Manoj, A. V., and Haripavan, N. (2022). Synthesis and characterization of mango leaves biosorbents for removal of iron and phosphorous from contaminated water. *Appl. Surf. Sci. Adv.* 11, 100292. doi:10.1016/j.apsadv.2022.100292

Elgarahy, A. M., Elwakeel, K. Z., Mohammad, S. H., and Elshoubaky, G. A. (2021). A critical review of biosorption of dyes, heavy metals and metalloids from wastewater as an efficient and green process. *Clean. Eng. Technol.* 4, 100209. doi:10.1016/j.clet.2021.100209

Elkhaleefa, A., Ali, I. H., Brima, E. I., Elhag, A. B., and Karama, B. (2020). Efficient removal of Ni(II) from aqueous solution by date seeds powder biosorbent: adsorption kinetics, isotherm and thermodynamics. *Processes* 8 (8), 1001. doi:10.3390/pr8081001

Elkhaleefa, A., Ali, I. H., Brima, E. I., Shigidi, I., Elhag, A. B., and Karama, B. (2021). Evaluation of the adsorption efficiency on the removal of Lead(II) ions from aqueous solutions using Azadirachta indica leaves as an adsorbent. *Processes* 9 (3), 559. doi:10.3390/pr9030559

Ettish, M. N., El-Sayyad, G. S., Elsayed, M. A., and Abuzalat, O. (2021). Preparation and characterization of new adsorbent from cinnamon waste by physical activation for removal of chlorpyrifos. *Environ. Challenges* 5, 100208. doi:10.1016/j.envc.2021.100208

FAOSTAT (2025). Available online at: https://www.fao.org/faostat/en/#data/QCL

Fito, J., Abewaa, M., Mengistu, A., Angassa, K., Ambaye, A. D., Moyo, W., et al. (2023). Adsorption of methylene blue from textile industrial wastewater using activated carbon developed from Rumex abyssinicus plant. *Sci. Rep.* 13 (1), 5427–17. doi:10.1038/s41598-023-32341-w

Foroutan, R., Jamaleddin Peighambardoust, S., Amarzadeh, M., Kiani Korri, A., Sadat Peighambardoust, N., Ahmad, A., et al. (2022). Nickel ions abatement from aqueous solutions and shipbuilding industry wastewater using ZIF-8-chicken beak hydroxyapatite. *J. Mol. Liq.* 356, 119003. doi:10.1016/j.molliq.2022.119003

Fu, C., Zhu, X., Dong, X., Zhao, P., and Wang, Z. (2021). Study of adsorption property and mechanism of lead(II) and cadmium(II) onto sulfhydryl modified attapulgite. *Arabian J. Chem.* 14 (2), 102960. doi:10.1016/j.arabjc.2020.102960

Futalan, C. M., Kim, J., and Yee, J. J. (2019). Adsorptive treatment *via* simultaneous removal of copper, lead and zinc from soil washing wastewater using spent coffee grounds. *Water Sci. Technol.* 79 (6), 1029–1041. doi:10.2166/wst.2019.087

Gutha, Y., Munagapati, V. S., Naushad, M., and Abburi, K. (2015). Removal of Ni(II) from aqueous solution by lycopersicum esculentum (tomato) leaf powder as a low-cost biosorbent. *Desalination Water Treat.* 54 (1), 200–208. doi:10.1080/19443994.2014.880160

Igwe, J. C., and Abia, A. A. (2007). Adsorption isotherm studies of Cd (II), Pb (II) and Zn (II) ions bioremediation from aqueous solution using unmodified and EDTA-Modified maize cob. *Eclética Quím.* 32 (1), 33–42. doi:10.1590/S0100-46702007000100005

Imran, M., Anwar, K., Akram, M., Shah, G. M., Ahmad, I., Samad Shah, N., et al. (2019). Biosorption of Pb(II) from contaminated water onto Moringa oleifera biomass: kinetics and equilibrium studies. *Int. J. Phytoremediation* 21 (8), 777–789. doi:10.1080/15226514.2019.1566880

Jang, M. H., and Hwang, Y. S. (2018). Effects of functionalized multi-walled carbon nanotubes on toxicity and bioaccumulation of lead in Daphnia magna. *PLoS One* 13 (3), e0194935. doi:10.1371/journal.pone.0194935

Junker-Frohn, L. V., Lück, M., Schmittgen, S., Wensing, J., Carraresi, L., Thiele, B., et al. (2019). Tomato's green gold: bioeconomy potential of residual tomato leaf biomass as a novel source for the secondary metabolite rutin. *ACS Omega* 4 (21), 19071–19080. doi:10.1021/acsomega.9b01462

Kalam, S., Abu-Khamsin, S. A., Kamal, M. S., and Patil, S. (2021). Surfactant adsorption isotherms: a review. *ACS Omega* 6 (48), 32342–32348. doi:10.1021/acsomega.1c04661

Khadim, A. T., Albayati, T. M., and Cata Saady, N. M. (2022). Removal of sulfur compounds from real diesel fuel employing the encapsulated mesoporous material adsorbent Co/MCM-41 in a fixed-bed column. *Microporous Mesoporous Mater.* 341, 112020. doi:10.1016/j.micromeso.2022.112020

Khan, I., Saeed, K., Zekker, I., Zhang, B., Hendi, A. H., Ahmad, A., et al. (2022). Review on methylene blue: its properties, uses, toxicity and photodegradation. *Water* 14 (2), 242. doi:10.3390/w14020242

Khodabandehloo, A., Rahbar-Kelishami, A., and Shayesteh, H. (2017). Methylene blue removal using Salix babylonica (weeping willow) leaves powder as a low-cost biosorbent in batch mode: kinetic, equilibrium, and thermodynamic studies. *J. Mol. Liq.* 244, 540–548. doi:10.1016/j.molliq.2017.08.108

Kumar, E., Bhatnagar, A., Hogland, W., Marques, M., and Sillanpää, M. (2014). Interaction of anionic pollutants with Al-based adsorbents in aqueous media – a review. *Chem. Eng. J.* 241, 443–456. doi:10.1016/j.cej.2013.10.065

Kumar, M., Nandi, M., and Pakshirajan, K. (2021). Recent advances in heavy metal recovery from wastewater by biogenic sulfide precipitation. *J. Environ. Manage* 278, 111555. doi:10.1016/j.jenvman.2020.111555

Largitte, L., and Pasquier, R. (2016). A review of the kinetics adsorption models and their application to the adsorption of lead by an activated carbon. *Chem. Eng. Res. Des.* 109, 495–504. doi:10.1016/j.cherd.2016.02.006

Lead in Food and Foodwares (2025). FDA. Available online at: https://www.fda.gov/food/environmental-contaminants-food/lead-food-and-foodwares

Lellis, B., Fávaro-Polonio, C. Z., Pamphile, J. A., and Polonio, J. C. (2019). Effects of textile dyes on health and the environment and bioremediation potential of living organisms. *Biotechnol. Res. Innovation* 3 (2), 275–290. doi:10.1016/j.biori.2019.09.001

Lin, L., Yang, H., and Xu, X. (2022). Effects of water pollution on human health and disease heterogeneity: a review. *Front. Environ. Sci.* 10, 880246. doi:10.3389/fenvs.2022.880246

Lupoi, J. S., Smith-Moritz, A., Singh, S., McQualter, R., Scheller, H. V., Simmons, B. A., et al. (2015). Localization of polyhydroxybutyrate in sugarcane using Fourier-transform infrared microspectroscopy and multivariate imaging. *Biotechnol. Biofuels* 8 (1), 98–99. doi:10.1186/s13068-015-0279-y

Ma, Z., Yang, Y., Wu, Y., Xu, J., Peng, H., Liu, X., et al. (2019). In-depth comparison of the physicochemical characteristics of bio-char derived from biomass pseudo components: Hemicellulose, cellulose, and lignin. *J. Anal. Appl. Pyrolysis* 140, 195–204. doi:10.1016/j.jaap.2019.03.015

Manzoor, K., Ahmad, M., Ahmad, S., and Ikram, S. (2019). Removal of Pb(II) and Cd(II) from wastewater using arginine cross-linked chitosan–carboxymethyl cellulose beads as green adsorbent. *RSC Adv.* 9 (14), 7890–7902. doi:10.1039/c9ra00356h

Martí, R., Roselló, S., and Cebolla-Cornejo, J. (2016). Tomato as a source of carotenoids and polyphenols targeted to cancer prevention. *Cancers* 8 (6), 58. doi:10.3390/cancers8060058

Marwani, H. M., Albishri, H. M., Jalal, T. A., and Soliman, E. M. (2017). Study of isotherm and kinetic models of lanthanum adsorption on activated carbon loaded with recently synthesized Schiff's base. *Arabian J. Chem.* 10, S1032–S1040. doi:10.1016/j.arabjc.2013.01.008

Mate, C. J., and Mishra, S. (2020). Synthesis of borax cross-linked jhingan gum hydrogel for remediation of remazol brilliant blue R (RBBR) dye from water: adsorption isotherm, kinetic, thermodynamic and biodegradation studies. *Int. J. Biol. Macromol.* 151, 677–690. doi:10.1016/j.ijbiomac.2020.02.192

Mosoarca, G., Vancea, C., Popa, S., Dan, M., and Boran, S. (2022). The use of bilberry leaves (Vaccinium myrtillus L.) as an efficient adsorbent for cationic dye removal from aqueous solutions. *Polymers* 14 (5), 978. doi:10.3390/polym14050978

Mubarak, M. F., Selim, H., and Elshypany, R. (2022). Hybrid magnetic core-shell TiO2@CoFe3O4 composite towards visible light-driven photodegradation of methylene blue dye and the heavy metal adsorption: isotherm and kinetic study. *J. Environ. Health Sci. Eng.* 20 (1), 265–280. doi:10.1007/s40201-021-00774-y

Mulla, B., Ioannou, K., Kotanidis, G., Ioannidis, I., Constantinides, G., Baker, M., et al. (2024). Removal of crystal violet dye from aqueous solutions through adsorption onto activated carbon fabrics. *C (Basel).* 10 (1), 19. doi:10.3390/c10010019

Nl Norme Libanaise Eau Potable Drinking Water (2025). Available online at: www.libnor.gov.lb

Pang, X., Sellaoui, L., Franco, D., Dotto, G. L., Georgin, J., Bajahzar, A., et al. (2019). Adsorption of crystal violet on biomasses from pecan nutshell, para chestnut husk, araucaria bark and palm cactus: experimental study and theoretical modeling *via* monolayer and double layer statistical physics models. *Chem. Eng. J.* 378, 122101. doi:10.1016/j.cej.2019.122101

Pavlović, D. M., Ćurković, L., Mandić, V., Macan, J., Šimić, I., and Blažek, D. (2021). Removal of pharmaceuticals from water by tomato waste as novel promising biosorbent: equilibrium, kinetics, and thermodynamics. *Sustainability* 13 (21), 11560. doi:10.3390/su132111560

Peydayesh, M., and Rahbar-Kelishami, A. (2015). Adsorption of methylene blue onto Platanus orientalis leaf powder: kinetic, equilibrium and thermodynamic studies. *J. Industrial Eng. Chem.* 21, 1014–1019. doi:10.1016/j.jiec.2014.05.010

Pham, V. H. T., Kim, J., Chang, S., and Bang, D. (2023). Investigating bio-inspired degradation of toxic dyes using potential multi-enzyme producing extremophiles. *Microorganisms* 11 (5), 1273. doi:10.3390/microorganisms11051273

Piepho, H. P. (2019). A coefficient of determination (R2) for generalized linear mixed models. *Biometrical J.* 61 (4), 860–872. doi:10.1002/bimj.201800270

Qasem, N. A. A., Mohammed, R. H., and Lawal, D. U. (2021). Removal of heavy metal ions from wastewater: a comprehensive and critical review. *npj Clean. Water* 4 (1), 36–15. doi:10.1038/s41545-021-00127-0

Radwan, E. K., Omar, R. A., and Moursy, A. S. (2023). Rapid adsorption of benzotriazole onto oxidized carbon cloth as an easily separable adsorbent. *Sci. Rep.* 13 (1), 17030–13. doi:10.1038/s41598-023-44067-w

Renu, M. A., Singh, K., Upadhyaya, S., and Dohare, R. K. (2017). Removal of heavy metals from wastewater using modified agricultural adsorbents. *Mater Today Proc.* 4 (9), 10534–10538. doi:10.1016/j.matpr.2017.06.415

Samuel, M. S., Shah, S. S., Bhattacharya, J., Subramaniam, K., and Pradeep Singh, N. D. (2018). Adsorption of Pb(II) from aqueous solution using a magnetic chitosan/graphene oxide composite and its toxicity studies. *Int. J. Biol. Macromol.* 115, 1142–1150. doi:10.1016/j.ijbiomac.2018.04.185

Sen, T. K. (2023). Adsorptive removal of dye (methylene blue) organic pollutant from water by pine tree leaf biomass adsorbent. *Processes* 11 (7), 1877. doi:10.3390/pr11071877

Sharma, J., Sharma, S., and Soni, V. (2023). Toxicity of malachite green on plants and its phytoremediation: a review. *Reg. Stud. Mar. Sci.* 62, 102911. doi:10.1016/j.rsma.2023.102911

Silva, V. C., Araújo, M. E. B., Rodrigues, A. M., Vitorino, MDBC, Cartaxo, J. M., Menezes, R. R., et al. (2021). Adsorption behavior of crystal violet and Congo red dyes on heat-treated Brazilian palygorskite: kinetic, isothermal and thermodynamic studies. *Materials* 14 (19), 5688. doi:10.3390/ma14195688

Singh, V., Ahmed, G., Vedika, S., Kumar, P., Chaturvedi, S. K., Rai, S. N., et al. (2024). Toxic heavy metal ions contamination in water and their sustainable reduction by eco-friendly methods: isotherms, thermodynamics and kinetics study. *Sci. Rep.* 14 (1), 7595–13. doi:10.1038/s41598-024-58061-3

Sultana, S., Munna, N., Sakib, T. U., Ahmed, N., Akanda, M. R., Saha, M. S., et al. (2024). High performance activated carbon derived from sawdust: preparation, characterizations, methyl Orange removal and kinetics investigation. *Biomass Convers. Biorefin* 15, 17295–17307. doi:10.1007/s13399-024-06422-3

Tam, C. C., Nguyen, K., Nguyen, D., Hamada, S., Kwon, O., Kuang, I., et al. (2021). Antimicrobial properties of tomato leaves, stems, and fruit and their relationship to chemical composition. *BMC Complement. Med. Ther.* 21 (1), 229. doi:10.1186/s12906-021-03391-2

Votat, S., Pontié, M., Jaspard, E., and Lebrun, L. (2024). Crystal violet (CV) biodegradation study in a dual-chamber fungal microbial fuel cell with Trichoderma harzianum. *Energies* 17 (1), 247. doi:10.3390/en17010247

Wan, S., Ma, Z., Xue, Y., Ma, M., Xu, S., Qian, L., et al. (2014). Sorption of lead(II), cadmium(II), and copper(II) ions from aqueous solutions using tea waste. *Ind. Eng. Chem. Res.* 53 (9), 3629–3635. doi:10.1021/ie402510s

Xiang, H., Min, X., Tang, C. J., Sillanpää, M., and Zhao, F. (2022). Recent advances in membrane filtration for heavy metal removal from wastewater: a mini review. *J. Water Process Eng.* 49, 103023. doi:10.1016/j.jwpe.2022.103023

Xu, L., Wu, C., Chai, C., Cao, S., Bai, X., Ma, K., et al. (2022). Adsorption of micropollutants from wastewater using iron and nitrogen co-doped biochar: performance, kinetics and mechanism studies. *J. Hazard Mater* 424, 127606. doi:10.1016/j.jhazmat.2021.127606

Yin, X. C., Liu, X., Fan, J. C., Wu, J. J., Men, J. L., and Zheng, G. S. (2017). Preparation of gel resins and removal of copper and lead from water. *J. Appl. Polym. Sci.* 134 (7). doi:10.1002/app.44466

Zhang, M., Wang, X., Yang, L., and Chu, Y. (2019). Research on progress in combined remediation technologies of heavy metal polluted sediment. *Int. J. Environ. Res. Public Health* 16 (24), 5098. doi:10.3390/ijerph16245098